Polarization effects in ionic systems from first principles

1993 J. Phys.: Condens. Matter 5 2687

(http://iopscience.iop.org/0953-8984/5/17/004)

J. Phys.: Condens. Matter 5 (1993) 2687–2706. Printed in the UK

Polarization effects in ionic systems from first principles

M Wilson and P A Madden
Physical Chemistry Laboratory, Oxford University, South Parks Road, Oxford OX1 3QZ, UK

Received 21 December 1992

Abstract. In this paper a classical application of the *Car–Parrinello* method in the computer simulation of ionic systems is demonstrated. The induction effects in the interionic interactions are included in addition to the short-range repulsion and dispersion effects described by effective pair potentials. By representing the induced dipoles as a pair of dynamically variable charges fixed on the ends of a rod and extending the Lagrangian accordingly, the self-consistent induced dipoles at each time step are generated from the values at the previous time step, without the need for explicit minimization. Coulomb-field-induced and overlap-induced polarization effects are included and these are parameterized by *ab initio* electronic structure calculations. For simple ionic systems it is shown that the neglect of the overlap-induced dipoles leads to a poor representation of real systems.

1. Introduction

Polarization effects (or induction forces) are normally incorporated into simulations of ionic systems via the shell model (see, for example, Sangster and Dixon [1] for a review). In the shell model an ion is represented by a core and a shell joined to it by a harmonic spring; the sum of the core and shell charges is the formal charge of the ion. The polarizability of the ion is parameterized by the shell charge and the force constant of the spring. In addition to the intercharge coulombic interactions the overlap and dispersion interactions, normally represented by a pair potential of the Born–Mayer (Fumi–Tosi) form, are considered to act on the shells. In this way dipoles induced by the Coulomb field *and* by short-range interactions are incorporated so that the induced dipoles are damped at short interionic separations where overlap effects become significant. The parameters are obtained by fitting to experimental data. At each time step the shells must be relaxed into the self-consistent energy minimum. This is usually done by an iterative steepest-descent method, but has recently been achieved by a conjugate-gradient procedure [2].

The most notable success of the shell model, over calculations using simple pairwise additive rigid-ion potentials, is in improving the phonon dispersion curves of ionic crystals [3]. In liquids, the dynamical behaviour is also affected. Besides lowering the frequencies of the high-frequency charge density wave oscillations (analogous to the optic phonons of the crystal), inclusion of the polarization effects alters diffusion coefficients [4]. The fluid structure is also influenced: the most notable feature is a decrease in the similarity of the like-pair distribution functions (g_{++} and g_{--}). In general the changes in fluid structure seem to improve the agreement with experimental data—especially where polarizable anions are involved [5]. However, even the shell models do not give good agreement with experiment in melts which involve highly polarizing (small) cations and polarizable anions, such as $MgCl_2$. The crystal structures of these systems are also difficult to rationalize on a simple ionic basis. In such cases 'covalency' is often invoked to explain the discrepancies, despite

0953-8984/93/172687+20$07.50

the fact that, on electronegativity grounds, these materials *ought* to be ionic. It seems to us worthwhile to explore whether such systems can be described with an ionic model (i.e. without invoking charge transfer) which allows for much stronger changes in the intrinsic properties of the ions due to environmental effects than are allowed for in the shell model.

The shell model, as normally used, seems to us a poor basis from which to attempt a more generalized description of polarization effects. The shell parameters are chosen empirically and the construct of representing the short-range induced dipoles as a consequence of a Born–Mayer interaction between shells seems to have no *a priori* justification. Furthermore, the normal shell model only reflects induced dipoles, whereas induced multipoles of higher-order must be involved in stabilizing the local structures of some of the target systems [6]. Higher-order multipoles occur in breathing shell models [7] but they arise as a side effect of allowing for environmental effects on the ion *polarizability* and their values are not well controlled. What is required is a computationally tractable model in which all aspects of the polarization phenomenon can be represented and parameterized on the basis of *ab initio* calculations.

In this paper we introduce a model which goes some way to fulfilling these objectives and show how it can be simulated inexpensively. The method avoids the self-consistent energy minimization process normally used in shell calculations, via a classical application of the Car–Parrinello (CP) method [8, 9]. In this way the self-consistent values of the induced multipoles at each time step in a molecular dynamics procedure are calculated from the values at the previous time step without the need for explicit minimization. Although most previous CP work has tended to concentrate on representing electronic effects directly and quantum mechanically via density functional theory (DFT) there is no reason why such a formalism could not be used in a classical sense. Indeed, Sprik [10, 11] has shown how it can be applied to model the permanent *and* induced dipoles in water in both a pure water system and in the study of the solvation of a chloride ion [12].

In the CP method we include our induced multipole moments as *additional* degrees of freedom via an extended Lagrangian formalism which enables us to systematically derive equations of motion for them. Thus the multipoles induced by both Coulomb fields (and their gradients) and short-range overlap effects may be seen to arise from a well-defined Hamiltonian in which the parameters may be fixed by electronic structure calculations of a type previously described [13].

Although, as outlined above, our target systems are the alkaline-earth halides and chalcogenides, in the present paper we restrict our attention to a careful description of the methodology and illustrate it in application to simple alkali halides.

2. The technique

2.1. The model

For the present, we envisage treating the polarization effects as an embellishment of a rigid-ion treatment; i.e. we imagine that short-range repulsion and also dispersion interactions are contained in an effective pair potential which acts between the ionic centres where the formal ion charges also reside. We mimic the induced multipoles with a set of variable charges at fixed separations from the ionic centre. Thus an induced dipole is represented by a rod of fixed length, free to rotate in space, with a pair of variable charges of equal magnitude but of opposite sign on its ends. The rod is chosen to be sufficiently short that higher-order multipoles are negligible. Thus the three degrees of freedom required to represent the components of the dipole are given by the charge magnitude, q, and the two

polar angles which specify the rod orientation. Higher-order multipoles can be represented by higher-order rigid polyhedra in the same way: for example, an ion with an induced dipole and quadrupole can be represented by an octahedron of variable charges with the constraint $\sum_{i=1}^{6} q_i = 0$; the requisite eight degrees of freedom being the five free charges and the three Euler angles necessary to specify the orientation of the octahedron. The reason for using a fixed framework and variable charges rather than the normal shell construct of charges on springs is to avoid the possibility of developing spurious (or uncontrolled) higher-order multipole moments because of over extension of the spring. For simplicity, in this work we restrict our attention to induced dipoles; the generalization to higher-order multipoles will be the subject of a future publication.

2.2. *Extending the Lagrangian*

In the CP method we include the variable charges and the angles defining the orientation of the polyhedron on which they sit as *additional* degrees of freedom via an extended Lagrangian formalism. The time derivatives of these extra variables, therefore, generate extra kinetic energy terms which we shall refer to as the 'fictitious' kinetic energy (FKE). The full kinetic energy, which contains the contribution from the translation of the ions as well as the FKE is:

$$T = \frac{1}{2}\sum_{i=1}^{N_t} m_i v_i^2 + \frac{1}{2} I_q \sum_{i=1}^{N_t} \omega_i^2 + \frac{1}{2} m_q \sum_{i=1}^{N_t}\sum_{\gamma=1}^{N_{sites}} \dot{q}_{i\gamma}^2 \tag{1}$$

where i labels the ion and $i\gamma$ labels the variable charge γ on ion i. N_t is the total number of ions in the system and N_{sites} is the number of variable charge sites per ion; since here we deal only with dipoles, N_{sites} will equal two. The mass of the ion is represented by m_i and the linear velocity by v_i. The angular velocity of the polyhedra is represented by ω_i and m_q is the inertia associated with the variation of the magnitude of the variable charges. I_q is the moment of inertia of the polyhedron. This 'mass' has no physical meaning but affords us the means of generating Newtonian equations of motion for the degrees of freedom of the additional terms. Notice also that the mass associated with the charge variation and that associated with the polyhedron rotation need not be the same.

The potential terms which involve the additional degrees of freedom are chosen by following ideas discussed by Sprik and Klein [10]. For induced dipoles only, the total potential energy ($\mathcal{U}$) is

$$\mathcal{U} = \sum_{i=1}^{N_t}\sum_{j=i+1}^{N_t} u(r_{ij}) + \frac{1}{2}\sum_{i=1}^{N_t} Q_i V^C(r_i) + \frac{1}{2}\sum_{i=1}^{N_t}\sum_{\gamma=1}^{2} V(r_{i\gamma}) q_{i\gamma} + \frac{1}{2} k_q \sum_{i=1}^{N_t}\sum_{\gamma=1}^{2} q_{i\gamma}^2 \tag{2}$$

where r_i labels the centre of the ion i and $r_{i\gamma}$ labels the variable charge γ on ion i. Here $u(r_{ij})$ is the short-range part of the normal ion–ion pair potential which includes the short-range repulsion due to overlap of the charge clouds and the dispersion interaction; it will typically be a Born–Mayer potential

$$u(r_{ij}) = B_{ij}\exp(-a_{ij} r_{ij}) - C_{ij}/r_{ij}^6 - D_{ij}/r_{ij}^8 \tag{3}$$

where the parameters B_{ij}, a_{ij}, C_{ij} and D_{ij} have their usual meaning [1]. The second term is the Coulomb energy of the formal charge Q_i on ion i, where $V^C(r_i)$ is the total Coulomb potential due to the formal and variable charges on the other ions at the centre of ion i

$$V^C(r_i) = \sum_{j\neq i}^{N_1} \left(\sum_{\nu=1}^{2} \frac{q_{\nu j}}{r_{ij\nu}} + \frac{Q_j}{r_{ij}} \right). \tag{4}$$

The third term in equation (2) involves a potential V acting on each fictitious charge. In the simplest case, where we require only the dipoles induced by the Coulomb interaction, $V(r_{i\gamma})$ would simply be the total Coulomb potential, $V^C(r_{i\gamma})$, at the site of the fictitious charge γ on ion i arising from *all* charges in the system except those belonging to the same ion: how V may be modified to allow for the overlap-induced dipoles will be discussed below. The final term in $\mathcal{U}$ is a purely intraion potential which gives the energy required to polarize the ion.

The equations of motion of these degrees of freedom may be derived by the procedures of Lagrangian mechanics ($\mathcal{L} = \mathcal{T} - \mathcal{U}$ is the Lagrangian). For the rotational motion it is straightforward to derive the usual rotational equations of motion for a rigid rod [15].

$$I_q \dot{\omega}_i = \tau_i \tag{5a}$$

$$\tau_i = -\frac{1}{2} \sum_{\gamma=1}^{2} d_{i\gamma} \times \nabla_{r_{i\gamma}} \mathcal{U} \tag{5b}$$

where $d_{i\gamma}$ is the vector from rod end to rod end on ion i and τ_i is the torque on rod i. These were integrated via a quaternion algorithm [16], a procedure that may be used when higher-order multipoles are involved.

For the charge variation, the Lagrange–Euler equation for charge $i\gamma$ now reads:

$$\frac{\mathrm{d}}{\mathrm{d}t} \frac{\partial \mathcal{L}}{\partial \dot{q}_{i\gamma}} - \frac{\partial \mathcal{L}}{\partial q_{i\gamma}} = 0 \qquad \gamma = 1, 2 \tag{6a}$$

$$m_q \ddot{q}_{i\gamma} = -k_q q_{i\gamma} - V(r_{i\gamma}). \tag{6b}$$

For each rod we have a pair of equations corresponding to $\gamma = 1, 2$. If we apply the constraint that $q_{i1} = -q_{i2} \equiv q_i$ and subtract the $\gamma = 2$ from the $\gamma = 1$ equation then:

$$m_q(\ddot{q}_{i1} - \ddot{q}_{i2}) = -k_q(q_{i1} - q_{i2}) - (V(r_{i1}) - V(r_{i2})) \tag{7}$$

or

$$m_q \ddot{q}_i = -k_q q_i - (V(r_{i1}) - V(r_{i2}))/2. \tag{8}$$

In order to see how this construct can represent the desired polarization effects we consider the simple case of pure Coulomb-field-induced dipoles. In this case the potential at the site of each rod-end charge, $V^C(r_{i1})$, can be found by Taylor expanding the total Coulomb potential about the ion centre, giving:

$$m_q \ddot{q}_i = -k_q q_i + E^C(r_i) \cdot d_i/2 \tag{9}$$

where $E^C(r_i)$ $(= -\nabla_{r_i} V^C(r_i))$ is the electric field at the centre of the ion and d_i is the vector joining the rod ends. For a given Coulomb potential the additional dynamical degrees

of freedom are at equilibrium when $\dot{\omega}_i$ and $\ddot{q}_i$ are zero. When this is true equations (9) and (5*b*) give

$$k_q q_i = \boldsymbol{E}^{\mathrm{C}}(\boldsymbol{r}_i) \cdot \boldsymbol{d}_i/2 \tag{10}$$

and

$$\boldsymbol{d}_i \times \boldsymbol{E}^{\mathrm{C}}(\boldsymbol{r}_i) = 0. \tag{11}$$

Hence, $\boldsymbol{d}_i$ is parallel to the electric field and the induced dipole $\boldsymbol{\mu}_i = q_i \boldsymbol{d}_i$ is given by:

$$\boldsymbol{\mu}_i = \boldsymbol{E}^{\mathrm{C}}(\boldsymbol{r}_i) d_i^2/2k_q. \tag{12}$$

If $d_i^2/2k_q$ is chosen to be equal to the ion polarizability, α, the induced dipole is given by $\alpha \boldsymbol{E}^{\mathrm{C}}(\boldsymbol{r}_i)$ and, as can be seen by substituting into equation (2), the induction energy is $-\frac{1}{2}\alpha(E^{\mathrm{C}}(\boldsymbol{r}_i))^2$. Both of these are the correct expressions for the ion polarization in an external field. If *all* dipoles satisfy this condition then the electric field that they generate will include the full self-consistent ion polarization effects. We denote the value of the field obtained when the condition is satisfied as $\bar{\boldsymbol{E}}^{\mathrm{C}}$. We dub this condition the *adiabatic condition* because, if it is satisfied during a dynamics run, the ion polarization will have the value required by the ion positions. When this condition holds, the dipoles on the ions will attain their full self-consistent values and the induction energy of the real system will be correct. The equations of motion for the ion positions read:

$$\frac{\mathrm{d}}{\mathrm{d}t}\frac{\partial \mathcal{L}}{\partial \dot{\boldsymbol{r}}_i} - \frac{\partial \mathcal{L}}{\partial \boldsymbol{r}_i} = 0 \tag{13a}$$

$$m_i \ddot{\boldsymbol{r}}_i = -\nabla_{\boldsymbol{r}_i} \mathcal{U} \tag{13b}$$

that is

$$m_i \ddot{\boldsymbol{r}}_i = -\sum_{j \neq i}^{N_i} \left[\nabla_{\boldsymbol{r}_i} u(r_{ij}) + Q_i \bar{\boldsymbol{E}}^{\mathrm{C}}(\boldsymbol{r}_i) + \boldsymbol{\mu}_i \cdot \nabla_{\boldsymbol{r}_i} \bar{\boldsymbol{E}}^{\mathrm{C}}(\boldsymbol{r}_i)\right] \tag{13c}$$

where we have Taylor expanded the potential about the centre of i and use $\boldsymbol{\mu}_i = q_i \boldsymbol{d}_i$. Consequently we see that the induced dipoles contribute to the induction forces on the ions in the correct way provided that the adiabatic condition holds.

2.3. Application of the Car–Parrinello method

The Car–Parrinello (CP) method of *ab initio* molecular dynamics [8, 9] is suggestive of a way of maintaining the adiabatic condition during an MD run. The additional degrees of freedom in the present calculation play a similar role to the coefficients in the expansion of the occupied orbitals in the electronic CP method [11]. We therefore anticipate that by integrating equations (5*b*), (9) and (13*c*) simultaneously, with the same (short) timestep appropriate for the internal degrees of freedom and starting from a configuration in which the adiabatic condition holds, then as the ions move the additional variables will be automatically updated to their new positions on the adiabatic surface.

We illustrate what happens when this procedure is applied in a run on liquid NaCl in figure 1(*a*). The details of the calculation will be given below. The figure shows a comparison of the induced dipoles on the ions with the value that this quantity should have

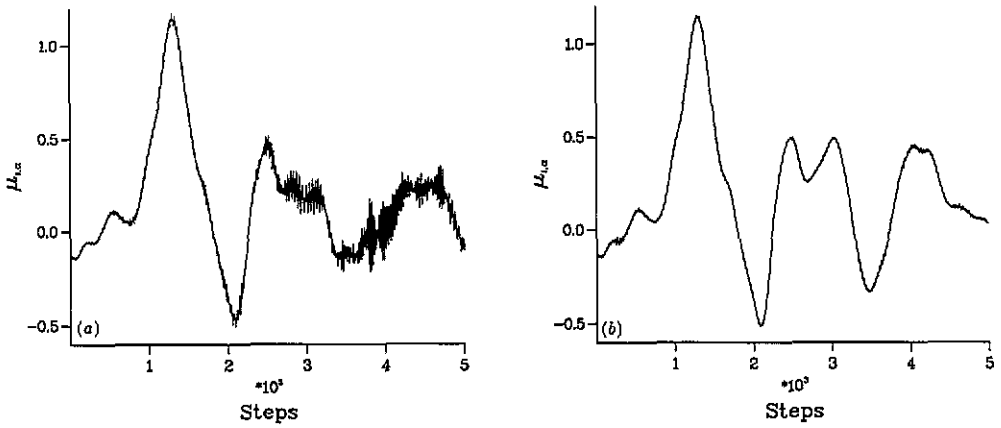

Figure 1. Evolution of the induced dipole on a randomly selected ion. The bold curve represents the required dipole (equation (14)) whist the lighter curve shows the dipole obtained via the polarizable model (*a*) without and (*b*) with thermostatting.

if the additional variables satisfied the adiabatic condition. The figure illustrates two points. Firstly, as the run progresses we see the instantaneous dipole oscillates more and more about the adiabatic value. Secondly, we see that the adiabatic value itself becomes increasingly oscillatory—this reflects the loss of adiabaticity in the dipoles on *other* ions which therefore make an erroneous oscillatory contribution to $\boldsymbol{E}^{\mathrm{C}}(\boldsymbol{r}_i)$. Thus, for a component of the dipole moment for an ion selected at random, we have

$$\mu_\alpha^i = \alpha E_\alpha^{\mathrm{C}}(\boldsymbol{r}_i) \tag{14}$$

against the value given by

$$\mu_\alpha^i = q_i d_{i,\alpha} \tag{15}$$

where α labels the x, y or z component. Figure 2(*a*) shows the evolution with time of the function

$$\Delta\mu_\alpha^i = \alpha E_\alpha^{\mathrm{C}}(\boldsymbol{r}_i) - q_i d_{i,\alpha} \tag{16}$$

which gives the departure of the instantaneous value from the adiabatic one. We see that, whilst the adiabatic condition is maintained for an appreciable period of time, eventually the magnitudes of the induced dipoles stray from the correct value and run out of control.

Another useful way of monitoring the adiabaticity in CP calculations is to monitor the fictitious kinetic energy (T_{FKE}). If the dynamics is proceeding smoothly with the adiabatic condition maintained, T_{FKE} will be small and its value will parallel the translational kinetic energy of the ions. This is because the only 'fictitious' motion is that required to update the additional variables as the ions move [9]. If the additional variables start to depart from their adiabatic values, T_{FKE} increases—this reflects a 'heating' of the additional variables by energy transfer from the ion translational motion. We illustrate this behaviour in figure 3 (upper curve, with the FKE represented as a temperature) for the same run as shown in figures 1(*a*) and 2(*a*). The slow, linear heating which is linked with the instability of the dipole values is clearly seen. Although the total energy of the extended system is conserved,

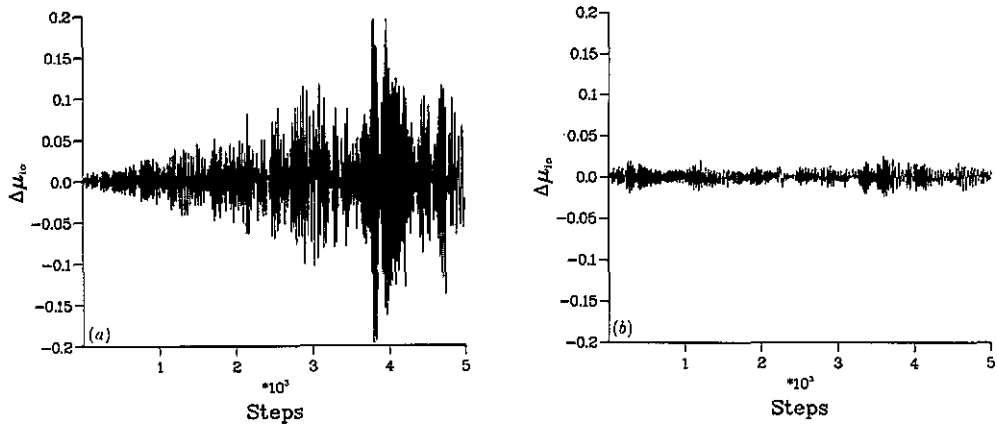

Figure 2. Evolution of $\Delta\mu_{i,\alpha}$ (equation (16)) with time for a system (*a*) without and (*b*) with thermostatting.

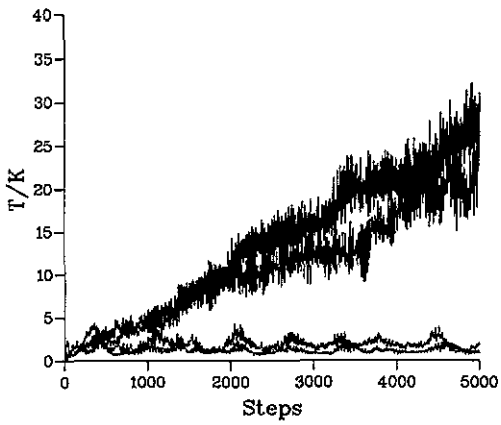

Figure 3. Evolution of the temperatures of the two fictitious systems (rotational and dynamic charge) with (upper curve) and without (lower) Nosé–Hoover thermostatting.

due to the transfer of energy from ion translation to the additional degrees of freedom, the sum of the kinetic and potential energies of the ions is not conserved.

The circumstances under which the electronic CP scheme can maintain the adiabatic condition for long periods has been discussed by Pastore *et al* [17]. If the character of the equations of motion of the additional variables is oscillatory and if the range of oscillation frequencies does not overlap the density of states of the translational degrees of freedom of the system studied, then energy transfer between the translational and additional degrees of freedom is slow and adiabaticity is maintained for long periods. In the electronic case, these favourable circumstances arise if there is an appreciable energy gap between the occupied and unoccupied electronic orbitals and if the fictitious inertia parameters are chosen sufficiently small. The converse occurs in metals, where there is no band gap. However, it has been shown [11, 18, 19] that in such cases a modified CP procedure, in which the excess heat transferred to the additional degrees of freedom is removed by adding 'thermostats' to the equations of motion, can maintain adiabaticity during long runs.

If we examine the equations of motion for the additional variables in the present calculation we see that they behave analogously to the metallic situation. Equation (9),

Table 1. NaCl potential parameters (in atomic units).

Ion pair	a	B_{ij}	C_{ij}	D_{ij}
+ +	1.6696	15.582	1.7549	2.9842
− −	1.6696	128.241	121.17	869.13
+ −	1.6696	46.168	11.699	51.850

for the variable charge behaves well, as any departure of the charge from the adiabatic value (equation (10)) will evolve with an oscillatory character. However, the equation of motion for the rod rotation equation (5*b*) is free rotational (in the absence of an external field); if this motion is heated, the rod will tend to spin freely. The behaviour of the system is therefore reminiscent of electronic CP simulations in metals and consequently we adopt the same corrective of applying Nosé–Hoover thermostats [20, 21] to the equations of motion of all degrees of freedom. The target temperature of the ion translational motion is the required physical temperature of the ionic system, that of the additional variables is a suitable low target value (see [18] for a discussion).

Figures 1(*b*) and 2(*b*) show that the character of the time evolution is influenced by the inclusion of thermostatting—they clearly show that the additional variables now adhere to their adiabatic values to within an acceptable degree of accuracy.

3. Details of the calculations

3.1. Thermostating the systems

Nosé–Hoover thermostats [20, 21] were employed on all three systems. Hence equation (13*c*) becomes:

$$m_i\ddot{\boldsymbol{r}}_i = -\sum_{j\neq i}^{N_t}\left[\nabla u(r_{ij}) + Q_i\bar{\boldsymbol{E}}^{\mathrm{C}}(\boldsymbol{r}_i) + \boldsymbol{\mu}_i\cdot\nabla_{\boldsymbol{r}_i}\bar{\boldsymbol{E}}^{\mathrm{C}}(\boldsymbol{r}_i)\right] - \zeta_{\mathrm{trans}}m_i\dot{\boldsymbol{r}}_i \tag{17}$$

where ζ_{trans} is the translational friction parameter. Similarly, equations (5*b*) and (9) now read:

$$\boldsymbol{\tau}_i = -\frac{1}{2}\sum_{\gamma=1}^{2}\boldsymbol{d}_{i\gamma}\times\nabla_{\boldsymbol{r}_{i\gamma}}\mathcal{U} - \zeta_{\mathrm{rot}}I_q\boldsymbol{\omega} \tag{18}$$

and

$$m_q\ddot{q}_i = -k_q q_i + \boldsymbol{E}^{\mathrm{C}}(\boldsymbol{r}_i)\cdot\boldsymbol{d}_i/2 - \zeta_{\mathrm{chg}}m_q\dot{q} \tag{19}$$

respectively. ζ_{rot} and ζ_{chg} are the friction parameters corresponding to the rotational motion and the change in the variable charges respectively. These parameters are updated as:

$$\dot{\zeta}_\beta = (T_{\mathrm{kin},\beta}/T_\beta - 1)/\tau_\beta^2 \tag{20}$$

where β labels the translational, rotational or variable charge motion. $T_{\mathrm{kin},\beta}$ is the kinetic temperature of the β-system, T_β is the target temperature, and τ_β is the characteristic thermostat relaxation time governing how 'harshly' the thermostat tries to keep $T_{\mathrm{kin},\beta} = T_\beta$. The parameters chosen will be given in the following section.

3.2. Choice of parameters

Tables 1–5 show the simulation parameters for all the runs discussed. The origin of the potential parameters will be discussed below. T_β is the target temperature for the subsystem β whilst $\langle T_\beta \rangle$ is the mean temperature of that subsystem over the duration of the simulation. The thermostat relaxation times, τ_β, are taken so as to provide acceptable temperature control whilst not allowing the equations of motion to become too stiff.

Table 2. LiF potential parameters (in atomic units).

Ion pair	a	B_{ij}	C_{ij}	D_{ij}
+ +	1.7696	3.6347	0.07625	0.1119
− −	1.7696	15.4524	15.1461	63.4132
+ −	1.7696	8.4501	0.8356	2.2381

Table 3. Polarizabilities (in atomic units).

	Li^+	Na^+	F^-	Cl^-
α	0.192	1.00	6.18	20.9

All simulations were performed with cubic periodic boundary conditions [22]. The long-range coulombic forces for all the permanent and variable charge interactions and the electric fields at the anion rod centres were calculated by means of the Ewald summation technique [22]. The Ewald parameter was chosen to be $\zeta = 5.0/L$, where L is the length of the side of the simulation cell. Around 180 k-points were used in the reciprocal space part of the summation. This introduces self-interaction terms between variable and permanent charges on the same ion. These were removed in the real-space part of the summation.

The translational and variable charge equations of motion were integrated via a leap-frog algorithm whilst the rotational equations were integrated via a quaternion algorithm.

3.3. Startup procedure

Starting from a given configuration of ionic coordinates, we require the self-consistent dipoles on each site. This can be achieved very simply by placing the rods on the ion sites and allowing them to relax under equations (5*b*) and (9) whilst keeping the ion positions frozen. When a maximum in the FKE is reached, the angular velocities and the charge velocities are quenched and relaxation restarted. The system approaches the self-consistent energy minimum through a series of such quenches. This is by no means the most efficient procedure for this kind of minimization but is very simple to program. Lindan and Gillan [2] have used a conjugate-gradient method to relax the massless shells in a shell model calculation.

3.4. Simulation timings

Table 6 shows some typical run times for the various modifications of the model described in this paper. All runs were performed on an IBM RISC 6000 320H with full preprocessing and optimization. The table shows whether only the anions or both the anions and cations were considered as polarizable. N_t is the total number of ions and hence $N_{charges}$ is the total number of charge sites in the system (i.e. three per polarizable ion). CF indicates whether current correlation functions were calculated 'on-the-fly'. The time given is for one complete time step.

Table 4. Simulation parameters for NaCl.

	Crystal		Liquid		
N_{steps}	10000	10000	10000	10000	10000
T_{trans} (K^{-1})	300	1073	1164	1224	1340
$\langle T_{trans}\rangle$ (K^{-1})	294.15	1077.44	1163.26	1223.41	1341.52
T_{rot} (K^{-1})	1.0	1.0	2.0	2.0	2.0
$\langle T_{rot}\rangle$ (K^{-1})	1.01	1.01	2.01	2.01	2.01
T_{chg} (K^{-1})	0.8	0.8	1.2	1.2	1.2
$\langle T_{chg}\rangle$ (K^{-1})	0.80	0.80	1.20	1.20	1.21
N	216	216	216	216	216
L (au^{-1})	31.9512	33.1498	35.9529	36.2923	36.9552
Δt (au^{-1})	20	20	20	20	20
d (au^{-1})	0.25	0.25	0.25	0.25	0.25
m_q^{chg}	5.0	5.0	5.0	5.0	5.0
m_q^{rot}	1000.0	1000.0	1000.0	1000.0	1000.0
τ^{trans}	10000.0	10000.0	10000.0	10000.0	10000.0
τ^{rot}	1000.0	1000.0	1000.0	1000.0	1000.0
τ^{chg}	1000.0	1000.0	1000.0	1000.0	1000.0

Table 5. Simulation parameters for LiF.

	Crystal		Liquid
N_{steps}	20000	20000	12000
T_{trans} (K^{-1})	100	100	1170
$\langle T_{trans}\rangle$ (K^{-1})	99.25	98.65	1169.24
T_{rot} (K^{-1})	1.0	1.0	5.0
$\langle T_{rot}\rangle$ (K^{-1})	1.00	1.01	4.99
T_{chg} (K^{-1})	0.4	0.4	0.5
$\langle T_{chg}\rangle$ (K^{-1})	0.39	0.39	0.49
N	216	216	216
L (au^{-1})	25.4699	25.4699	26.1236
Δt (au^{-1})	12	12	10
d (au^{-1})	0.25	0.25	0.25
m_q^{chg}	5.0	5.0	5.0
m_q^{rot}	1000.0	1000.0	1000.0
τ^{trans}	10000.0	10000.0	10000.0
τ^{rot}	1000.0	1000.0	1000.0
τ^{chg}	1000.0	1000.0	1000.0

Table 6. Typical run times for three modifications of the model and the RIM using the same optimization procedures.

	N_t	α_+	α_-	$N_{charges}$	CF	Time
RIM	216	×	×	216	√	1.58
PM	216	×	√	432	×	3.91
PM	216	×	√	432	√	4.28
PM	216	√	√	648	√	8.19

4. Polarization effects in NaCl and LiF

The specification of the interion interaction-potential can be considered in two stages. In a

perfect cubic crystal the Coulomb field at the site of the ion vanishes by symmetry. Hence, induction effects do not contribute to the properties of a perfect crystal. The Born–Mayer potential includes only the overlap-mediated repulsion and dispersion terms besides the charge–charge Coulomb potential. The properties of the perfect crystal are sufficient to determine the parameters required. The lattice parameter, compressibility and expansion coefficient are used as input to determine the Fumi–Tosi parameter set. In a vibrating or disordered crystal, or in the melt, however, the induction forces become non-zero. We are interested in exploring the postulate that in such systems the short-range and dispersion interactions between the ions should take the same values as those determined for the crystal, leaving the only parameters to be fixed as those which control the ionic polarization. By building a description of the polarization on the basis of *ab initio* electronic structure calculations on the crystal we hope to identify unambiguously those aspects which determine particular observable properties. In this section we neglect the dipoles induced by the short-range interionic interactions so that the parameters required are simply ionic polarizabilities. Consistent with the above postulate we take these ionic polarizabilities to be the in-crystal values calculated *ab initio* by Fowler and Madden [13]. We note that studies of interaction-induced light scattering from ionic melts has confirmed the essential similarities of the ionic polarizabilities in the crystal and melt, at least for the alkali halides [23, 24, 25].

Of course, it would be desirable to establish *all* the potential parameters *ab initio*. Pyper [14] has reviewed the progress which has been made in this direction. For the alkali halides the *ab initio* potentials which emerge agree well with the Fumi–Tosi ones. This indicates that the Born–Mayer form captures the essential features required in a cubic crystal and that, for crystals of such high symmetry, the crystal properties are sufficient for an empirical parameterization. We have used the Fumi–Tosi potentials to simplify the comparison with previous work. We note that for other materials, which crystallize in lower symmetry, potentials have been parameterized on other types of data, such as lattice energies and defect formation energies, and that the accord with *ab initio* potentials is then often poorer.

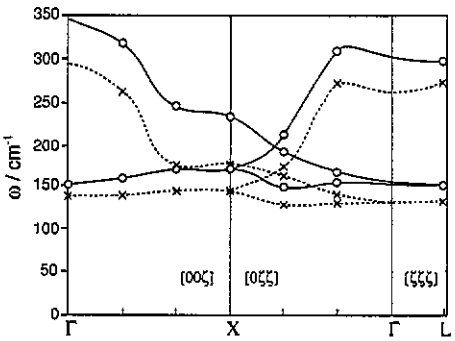

Figure 4. Phonon dispersion curve for NaCl at 300 K. Crosses correspond to the model which includes the Coulomb-field-induced dipoles only, whilst the circles are for an RI simulation under the same conditions.

In this section we survey the extent to which the inclusion of polarization effects, neglecting any dipoles induced by short-range interactions, improves the representation of simple ionic systems over the rigid ion model, i.e. the simple Fumi–Tosi potential (RIM).

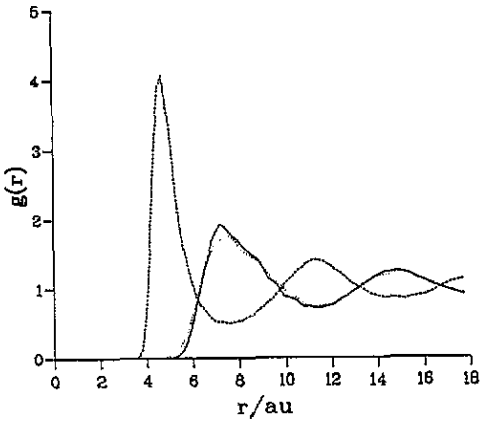

Figure 5. Radial distribution functions for the NaCl system from the polarizable model. ——, $g_{ClCl}(r)$; - - - -, $g_{NaCl}(r)$; · · · · · ·, $g_{NaNa}(r)$.

4.1. Crystalline NaCl

The well-known effect of ionic polarization in a vibrating crystal is to reduce the splitting of the longitudinal and transverse optic bands. In a primitive model of the crystal the splitting at the Brillouin zone centre is given by

$$\omega_{LO}^2 - \omega_{TO}^2 = 4\pi\rho e^2/\epsilon_\infty \tag{21}$$

where ρ is the ion-pair number density, e the electronic charge and ϵ_∞ the high frequency dielectric permittivity. For unpolarizable ions $\epsilon_\infty = 1$, whereas for crystalline NaCl $\epsilon_\infty = 2.2$ [26].

Figure 4 shows the optical components of the phonon dispersion curve calculated from the longitudinal and transverse charge current correlation functions for the RIM and for the polarizable model described above. Jacucci *et al* [4] have previously compared RIM and shell model dispersion curves for this system. We see that the LO–TO splitting has been reduced by including the induction effects. However, the improvement in agreement with the experimental dispersion curves over the RIM is not as good as that obtained by Jacucci *et al* (see figure 3 of [4]). If we focus on the [00ζ] branch we see that both the LO and TO frequencies seem to be down-shifted uniformly between the Γ point and the zone boundary. In the shell model calculations the TO phonons appear at similar frequencies to the RIM whereas the LO phonons are down-shifted at the zone centre and barely changed at the zone boundary. We will see later that including overlap-induced dipoles substantially improves this situation.

4.2. Molten NaCl

Figures 5 and 6 show the partial radial distribution functions for the rigid ion and the polarizable model. The same interaction potentials were used in the simulation of molten NaCl; the physical conditions are given in table 4. The most striking effect is seen to be the broadening and inward shifting of the first peak in g_{++} and the inward shift and reduction in height of g_{+-}. A reduction in the similarity of g_{++} and g_{--} with respect to the RIM seems to be indicated by experimental data [27] (a detailed comparison is shown in figures 15 and 16 of [1]). However, the inward shift of g_{++} does seem to be more pronounced in the polarizable model than is observed experimentally. Overall, it seems as if the general changes in the fluid structure as a result of including induction effects are in the direction

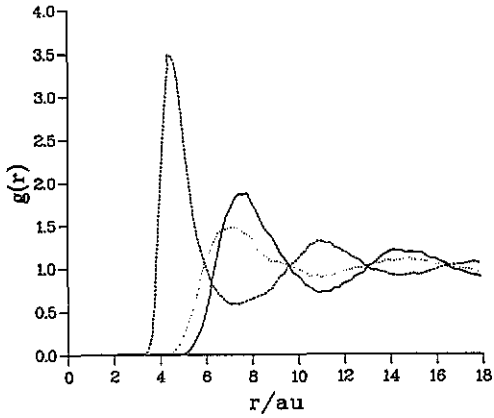

Figure 6. Radial distribution functions for the NaCl system from the RIM. ——, $g_{ClCl}(r)$; - - - -, $g_{NaCl}(r)$; ·····, $g_{NaNa}(r)$.

Table 7. Na^+ diffusion coefficients compared with previous RI simulation and experimental results (in units of 10^{-5} cm^2 s^{-1}).

T (K^{-1})	Polarizable model	RI model	Experiment
1173	12.2	9.7	11.1
1224	15.2	10.8	13.1
1340	18.2	14.1	17.3

Table 8. Cl^- diffusion coefficients compared with previous RI simulation and experimental results (in units of 10^{-5} cm^2 s^{-1}).

T (K^{-1})	Polarizable model	RI model	Experiment
1173	10.1	8.6	8.0
1224	10.4	9.8	9.6
1340	16.1	12.2	12.9

indicated by experiment but that the magnitude of these changes is too large in the absence of short-range induced dipoles.

Tables 7 and 8 show diffusion coefficients calculated from the gradient of the mean-square displacement in the linear region for Na^+ and Cl^- respectively. Also shown is data for a rigid-ion simulation [28] and experiment [29]. Both the cation and anion values are systematically higher than experiment.

Figure 7 shows the behaviour of the induction energy of the system for various statepoints (i.e. the total energy associated with the ionic polarizability) with the experimental melting temperature, T_m shown for comparison. This emphasizes the important role of the induction terms in the thermodynamics of melting.

4.3. Molten LiF

We also attempted a simulation of molten LiF with a polarizable potential (neglecting short-range induced dipoles). We omitted the very small lithium cation polarizability in this model. This calculation failed in the sense that anions and cations were found to approach to unphysically short separations (this does not occur with the RIM). The origin of this problem is the fact that the lithium cations have small ionic radii and can make close approaches to the fluoride anions in the melt; in the polarizable model this results in the induction of

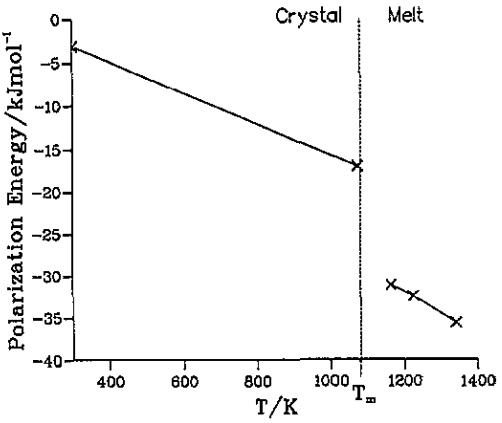

Figure 7. Polarization energy of NaCl at a series of statepoints.

very large dipoles and consequently very large attractive induction forces which overcome the short-range repulsion in the Fumi–Tosi potential.

5. Dipoles induced by short-range interactions

The above results indicate that the simple model of polarization effects, in which the induced dipoles are calculated from the Coulomb field at the centre of the ion, has significant shortcomings. In particular it appears not to describe correctly the effects of ionic polarization on the coulombic interactions in crystals and can break down for typical ion configurations in the melt—the ions become over-polarized. The model neglects the dipoles induced by short-range overlap effects—which should oppose the Coulomb-field-induced dipoles (at least for cation–anion contacts). In the shell-model account of ionic polarization, the short-range damping of the induced dipoles is handled by placing the site of the short-range potential (u_{ij}) on the shell charge, rather than at the centre of mass of the ion. This *ad hoc* procedure links the magnitude of the overlap-induced dipoles to the interionic potential in a way which is overly restrictive and can lead to difficulties in parameterization.

Fowler and Madden [30] investigated the short-range induced dipole (i.e. the part of the dipole not induced by the Coulomb field and its gradient) in a series of electronic structure calculations on distorted LiF crystals. They demonstrated that it could be viewed as the result of an additional potential (dubbed the 'dent-in-the-wall term') and that the effect of several ions was approximately additive. These findings suggest that these dipoles can be incorporated into the present model by adding a term to V^C in equation (4), i.e. we write

$$V(\boldsymbol{r}_{i\gamma}) = V^C(\boldsymbol{r}_{i\gamma}) + \sum_{j\neq i}^{N_l} f(r_{ij}) \frac{Q_j}{r_{i\gamma j}} \tag{22}$$

where $f(r)$ is a suitable short-range function which will be chosen to take a limiting value of -1 as $r \to 0$ and to reproduce the *ab initio* dipoles calculated by Fowler and Madden when r is in the range of nearest-neighbour separations. By following the same argument used to link the induced dipole to the Coulomb field (equations (9)–(11)) it is straightforward to show that, at the adiabatic condition, the induced dipole will now be:

$$\boldsymbol{\mu}_i = \alpha \boldsymbol{E}^C(\boldsymbol{r}_i) + \sum_{j\neq i}^{N_l} \alpha f(r_{ij}) \frac{Q_j \boldsymbol{r}_{ij}}{|\, r_{ij}^3 \,|}. \tag{23}$$

By choosing this form for the short-range potential and an appropriate small-r limiting behaviour of $f(r)$ we ensure that the short-range term cancels the Coulomb effects if two ions should approach to unphysical separations—this should prevent the kind of catastrophic overpolarization found in the LiF calculations discussed above and would mean that the induced dipoles at physical separations include both the Coulomb-field and overlap-induced dipoles correctly.

A convenient form for $f(r)$ was introduced by Tang and Toennies [31] as a damping function for dispersion forces; we set

$$f(r_{ij}) = -\exp(-br_{ij}) \sum_{k=0}^{4} \frac{(br_{ij})^k}{k!} \tag{24}$$

which has the properties outlined above and determine the sole parameter b for LiF by requiring that the dipole obtained from equation (23) for a distorted crystal agree with those calculated by Fowler and Madden [13, 32]. The value for b obtained in this way is 1.0835au.

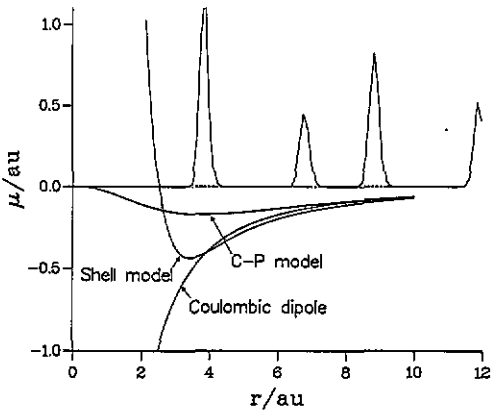

Figure 8. Comparison of the induced dipole moment for a cation–anion pair for pure Coulomb-field induction, in the shell model and with the *ab initio* parameterized model (equations (23) and (24)). The crystal $g_{NaCl}(r)$ function is superimposed in order to judge the range of the effect.

In figure 8 we compare the magnitude of the dipole induced in a fluoride ion when a lithium ion approaches it; we use the in-crystal F^- polarizability and the short-range function f chosen to fit the *ab initio* short-range, in-crystal induced dipoles as discussed above. Also shown in the figure is the cation–anion radial distribution function for molten LiF (RIM) and the dipole induced by the interionic Coulomb field (as in the polarization model discussed in section 2). We see that the modification of the induced dipole in the range of nearest-neighbour separations is dramatic. Note too that, by virtue of the form of f, the total induced dipole is quenched when the ions make close approaches—within the range of the sum of ionic radii; this should prevent the overpolarization effect found when the short-range term is ignored. We also show in figure 8 the induced dipole which would be obtained in the shell model (with the parameters given by Sangster and Dixon [1]). At long range, the induced dipoles are in reasonable agreement (this reflects the fact that the ion polarizability implicit in the shell potential is close to the *ab initio* value (6.90 versus 6.18 au)). At short range, the shell-model dipole also includes a term due to the spring extension caused by the force exerted on the shell by the short-range (Fumi–Tosi) potential. We see that the major beneficial effect of this term is to damp and even reverse the sign of the dipole, relative to the Coulomb-field-induced term. This means that the

induction force between the ions will switch from being attractive to repulsive when the ions approach closely and prevent the overpolarization effects noted above. However, we see that the dipoles predicted by this *ad hoc* representation of the short-range effects leads to values for the induced dipoles in the nearest-neighbour regime which are completely at variance with the *ab initio* values. Note also that the damping is still significant at the second-nearest cation level. A distorted crystal calculation at this distance gives a value of the total dipole of 1.7% different from the purely coulombic value compared with 2% from Fowler and Madden [30].

With the inclusion of the additional term, the third term in the potential energy function (equation (2)) now reads:

$$\frac{1}{2}\sum_{i=1}^{N_t}\sum_{\gamma=1}^{2} q_{i\gamma}\left(V^{C}(\boldsymbol{r}_{i\gamma})+\sum_{j\neq i}^{N_t} f(r_{ij})\frac{Q_j}{r_{i\gamma j}}\right). \tag{25}$$

The extra term, therefore, leads to extra forces and torques in addition to those included in equations (5*b*), (9) and (13*c*). Specifically, equation (9) becomes:

$$m_q\ddot{q}_i = -k_q q_i + \frac{\boldsymbol{E}^{C}(\boldsymbol{r}_i)\cdot\boldsymbol{d}_i}{2} + \sum_{j\neq i}^{N_t}\frac{\boldsymbol{r}_{ij}}{|\,r_{ij}^3\,|} f(r_{ij})Q_j \tag{26}$$

equation (5*b*) becomes:

$$\boldsymbol{\tau}_i = -\frac{1}{2}\sum_{\gamma=1}^{2}\boldsymbol{d}_{i\gamma}\times\nabla_{\boldsymbol{r}_{i\gamma}}\mathcal{U} + \sum_{j\neq i}^{N_t}\boldsymbol{\mu}_i\times f(r_{ij})\frac{Q_j\boldsymbol{r}_{ij}}{|\,r_{ij}^3\,|}Q_j \tag{27}$$

and there is an extra force term in equation (13c) given by:

$$\frac{\mu_\alpha f(r_{ij})}{|\,r_{ij}^3\,|}q_j + \boldsymbol{\mu}_i\cdot\boldsymbol{r}_{ij}\left(\frac{-3r_{i,\alpha}f(r_{ij})}{|\,r_{ij}^5\,|}+\frac{r_{i,\alpha}}{|\,r_{ij}^4\,|}\frac{df(r_{ij})}{dr_{ij}}\right). \tag{28}$$

We will now demonstrate the effect of including the overlap-induced dipoles on the properties of LiF.

5.1. Crystalline LiF

Figure 9 shows the phonon dispersion curve for LiF along the three main high-symmetry directions for both the polarizable model and the RIM. We note that th LO–TO splitting has been greatly reduced. We note also that the (100) TO mode is now raised with respect to the TO from the RIM calculation. This is the opposite of the effect seen in the NaCl calculation of section 4.1 where only Coulomb-field-induced dipoles were considered. This raising of the TO mode is consistent both with experiment and previous shell-model calculations.

Figure 10 shows the phonon dispersion curve along the (100) direction only for the full polarizable model, the RIM, and a polarizable model with the short-range parameter $b = 2.0$ providing an extreme short-range damping to prevent catastrophic overpolarization but reproducing the Coulomb-field-induced dipoles at physical separations. We note that the effect of the short-range function on the short-wavelength LO mode and the whole TO mode is dramatic. In the TO case the mode is lowered with respect to the RIM as was seen earlier for NaCl. Therefore, we postulate that if the short-range effects were included in

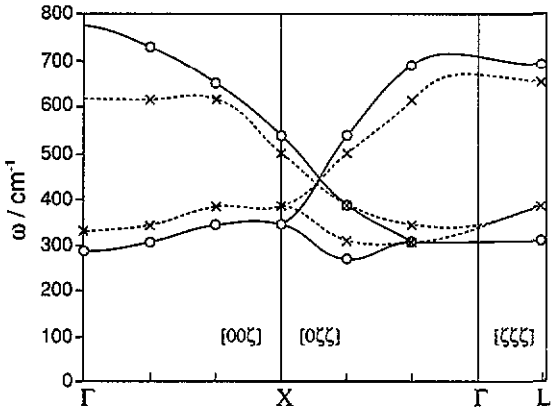

Figure 9. Phonon dispersion curves for LiF at 100 K from the RIM and polarizable models.

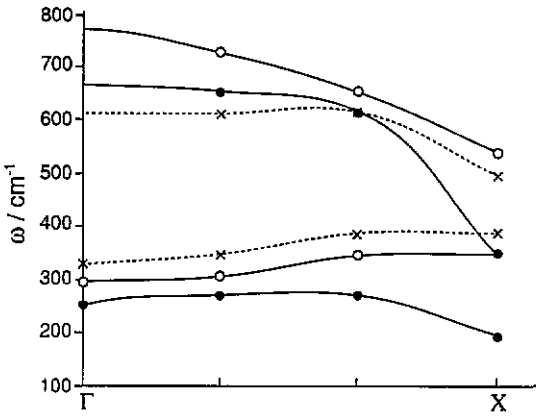

Figure 10. Phonon dispersion curves for LiF at 100 K along the (100) direction from the RIM (open circles), polarizable model with full short-range contributions (crosses) and the polarizable model with a much reduced short-range contribution (full circles).

our model the TO mode would be raised and thus the LO–TO splitting would be consistent with experiment.

The varying influence of the short-range dipoles across the Brillouin zone can be understood in the following way. We need to think of the energetics of a distortion of the charge density at different wavelengths. At the zone boundary, adjacent anions and cations are displaced in opposite directions and the dominant source of the induced dipoles is this nearest-neighbour displacement. We have seen (figure 8) that the Coulomb-field-induced dipole at the nearest-neighbour separations is much larger than in reality due to the opposing overlap-induced term. Hence, in the absence of the short-range term, the effect of the ionic polarizability on the energetics of lattice distortions at the zone boundary will be overestimated. Closer to the zone centre, the relevant ionic interactions will be relatively long ranged and adequately described by the simple Coulomb model.

5.2. Molten LiF

In figures 11 and 12 we compare the radial distribution functions for molten LiF calculated with the full, *ab initio* parameterized polarization model described above with those obtained from the RIM simulations at the same statepoint. We note that the excessive effects of the ionic polarization on the liquid structure, found when the overlap-induced dipoles were

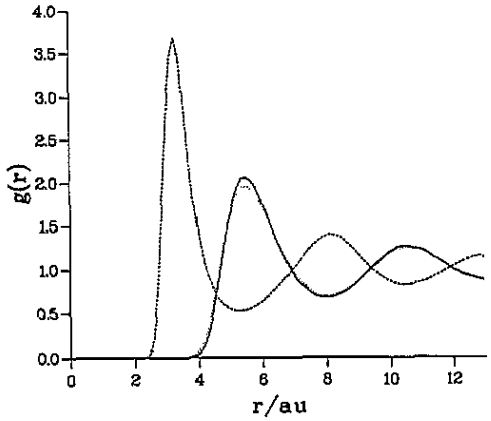

Figure 11. Radial distribution function for molten LiF from the polarizable model with full short-range dipole contributions. ——, $g_{ClCl}(r)$; - - - -, $g_{NaCl}(r)$; · · · · · ·, $g_{NaNa}(r)$.

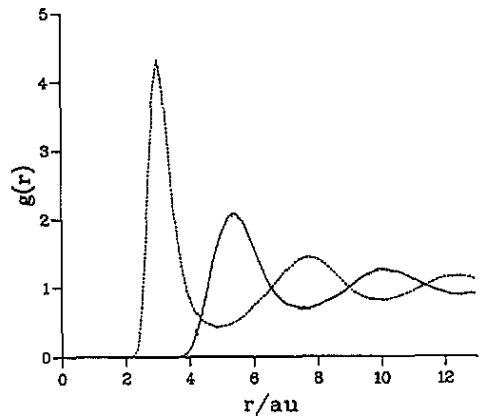

Figure 12. Radial distribution function for molten LiF from the RIM. ——, $g_{ClCl}(r)$; - - - -, $g_{NaCl}(r)$; · · · · · ·, $g_{NaNa}(r)$.

neglected (i.e. the instability of the LiF simulations and the marked shifts in g_{+-} and g_{++} in NaCl, have now disappeared). This is because the net induced dipoles arising from first-neighbour cation–anion interactions have been greatly reduced (see figure 8). The radial distribution functions resemble the RIM ones quite closely, the only significant effect appears to be an increase in the height and inward shift of g_{+-}. Since there is no experimental data on the structure of molten LiF we cannot confirm these findings directly. However, in NaCl we noted that the inward shift of g_{++} with respect to the RIM result, from the coulombic induction effects, did not seem to be confirmed by experiment [27] (although g_{++} did seem to be broader than g_{--}), and that the experimental results seemed to indicate a lower peak in g_{+-} than found in the RIM. Since NaCl has a more polarizable anion than LiF we might anticipate that the structure we would find in this case would be intermediate between the RIM and the purely coulombic induction model and hence in better agreement with experiment than either.

The diffusion coefficients, again calculated from the ion mean square displacement functions were found to be $D_+ = 8.2 \times 10^{-5}$ cm^2 s^{-1} and $D_- = 6.3 \times 10^{-5}$ cm^2 s^{-1} compared with the RIM values of 10.1 and 8.8, respectively. Thus, the ions appear to be moving more slowly in the polarizable model. We note that such a finding is consistent with earlier shell-model calculations on LiCl [23].

6. Conclusion

We have shown how *ab initio* parameterized representations of induced dipoles can be incorporated into the interionic force field used in simulations of ionic systems in a computationally tractable way. This is achieved by a classical adaptation of the Car–Parrinello method. The dipoles are fully self-consistent and so include the many-body aspects of the induction forces. We have indicated how the method can be generalized to deal with higher-order induced multipoles. The dipoles induced by both the interionic Coulomb-field and the short-range overlap effects may be included.

The method was applied to the relatively simple examples of LiF and NaCl; the phonon dispersion curves in the crystal and radial distribution functions for the melt were examined. The parameters which determine the induced dipoles were taken from electronic structure calculations on crystals. We have showed that the values of the short-range dipoles captured in the shell model differ markedly from the *ab initio* values. Neglect of the overlap-induced dipoles had catastrophic consequences for LiF, where the cations and anions tended to collapse onto each other under the influence of the induction forces. In the crystal the expected improvement in the LO–TO splitting over rigid-ion simulations (RIM) was obtained; for small wavevectors the inclusion of the short-range dipoles appeared to have little effect and the zone boundary splitting was close to the value expected from the Lyddane–Sachs–Teller expression, modified for the high-frequency dielectric constant. At higher wavevectors, the dispersion relationship predicted with and without the short-range terms differed appreciably. Unfortunately, we were unable to find experimental data for LiF with which to compare these findings in detail. In the liquid, we found appreciable differences between the radial distribution functions obtained for NaCl with the rigid-ion model when the Coulomb-field induction was included. In particular, there was a marked inward shift and broadening of the first peak of g_{++}; the experimental results appear to show that this tendency is too strong. The overlap-induced dipoles correct this problem and restore the radial distribution functions to closer similarity with the RIM results (at least in LiF).

We cannot claim that the model for the induction effects we have employed is fully vindicated by experimental findings. The experimental data for LiF, for which we have a full *ab initio* model, is not sufficiently complete for a full comparison. For NaCl, for which more data is available, we do not have a model for the overlap-induced dipoles. We are presently working to improve this situation in two respects. Firstly, the properties of the induced dipoles may be observed *directly* in far-infrared spectroscopy (and the induced dipoles also contribute to the frequency-dependent conductivity). Data on both these properties are available for molten LiF and we will present a comparison with simulation results shortly. Secondly, we are developing interaction potential models for a wider range of more-polarizable alkali and alkaline-earth halides with the aid of further electronic structure calculations; these will form the basis of wide-ranging structural and dynamical studies.

Acknowledgments

MW would like to thank SERC and the Royal Signals and Radar Establishment (RSRE) Malvern for CASE award No 91565144. The authors would like to thank SERC for grant No GR/H10276 allowing the purchase of two IBM series 6000 320H machines on which all the calculations in this work were performed.

References

[1] Sangster M J L and Dixon M 1976 *Adv. Phys.* **23** 247–342
[2] Lindan P J D and Gillan M J 1993 *J. Phys.: Condens. Matter* **5** 1019
[3] Cowley R A, Cochran W, Brockhouse B N and Woods A D B 1963 *Phys. Rev.* **131** 1030
[4] Jacucci G, McDonald I R and Rahman A 1976 *Phys. Rev.* A **13** 1581
[5] Dixon M and Gillan M J 1981 *Phil. Mag.* B **43** 1099
[6] Harrison N M and Saunders V R 1992 *J. Phys.: Condens. Matter* **4** 3873
[7] Schröder U 1966 *Solid State Commun.* **4** 347
[8] Car R and Parrinello M 1985 *Phys. Rev. Lett.* **55** 2471
[9] Remler D K and Madden P A 1990 *Mol. Phys.* **70** 921–66
[10] Sprik M and Klein M L 1981 *J. Chem. Phys.* **89** 7556–66
[11] Sprik M 1991 *J. Phys. Chem.* **95** 2283–91
[12] Sprik M 1993 *Computer Simulation in Chemical Physics* ed M P Allen and D J Tildesley (Berlin: Kluwer) p 211
[13] Fowler P W and Madden P A 1984 *Phys. Rev.* B **29** 1035
[14] Pyper N C 1991 *Adv. Solid State Chem.* **2** 223
[15] Goldstein H 1980 *Classical Mechanics* (Reading, MA: Addison-Wesley)
[16] Evans D J and Murad S 1977 *Mol. Phys.* **34** 327–31
[17] Pastore G, Smargiassi E and Buda F 1991 *Phys. Rev.* A **44** 6334
[18] Fois E F, Madden P A and Penman J I 1991 *Advances in Biomolecular Simulation* ed R Lavery, J-L Rivail and J Smith (New York: American Institute of Physics)
[19] Blöchl P E and Parrinello M 1992 *Phys. Rev.* B **45** 9413
[20] Nosé S 1984 *Mol. Phys.* **52** 255; 1984 *J. Chem. Phys.* **81** 511
[21] Hoover W G 1985 *Phys. Rev.* A **31** 1695
[22] Allen M P and Tildesley D J 1987 *Computer Simulation of Liquids* (Oxford: Clarendon)
[23] O'Sullivan K F and Madden P A 1991 *J. Phys.: Condens. Matter* **3** 8751
[24] Madden P A, O'Sullivan K F, Board J A and Fowler P W 1991 *J. Chem. Phys.* **94** 918
[25] O'Sullivan K F 1990 *DPhil Thesis* Oxford University, unpublished
[26] March N H and Parrinello M 1982 *Collective Effects in Solids and Liquids* (Brighton: University of Sussex Press)
[27] Edwards F G, Enderby J E, Howe R A and Page D I 1975 *J. Phys. C: Solid State Phys.* **8** 3483
[28] Ciccotti G, Jacucci G and McDonald I R 1976 *Phys. Rev.* A **13** 426
[29] Young R E and O'Connell J P 1971 *Ind. Eng. Chem. Fundam.* **10** 418
[30] Fowler P W and Madden P A 1985 *Phys. Rev.* B **31** 5443
[31] Tang K T and Toennies J P 1984 *J. Chem. Phys.* **80** 3726
[32] Fowler P W private communication